Submitted to Colloids and Surfaces A

Deposition of silica nanoparticles onto alumina measured by optical reflectometry and quartz crystal microbalance with dissipation techniques

Hasan Guleryuz [a], Ingeborg Kaus [b], Cédric C. Buron [c], Claudine Filiâtre [c], Niklas Hedin [d], Lennart Bergström [d], Mari-Ann Einarsrud [a] *

[a] Department of Materials Science and Engineering, Norwegian University of Science and Technology, 7491 Trondheim, Norway
[b] SINTEF Materials and Chemistry, 7465 Trondheim, Norway
[c] Institut UTINAM UMR CNRS 6213, Université de Franche-Comté, 25030 Besançon, France
[d] Department of Materials and Environmental Chemistry, Stockholm University, 2011, Stockholm, Sweden

**Corresponding author*
Mari-Ann Einarsrud
Department of Materials Science and Engineering, Norwegian University of Science and Technology, 7491 TRONDHEIM
Phone: +47 735 94002, Fax:+47 735 50203
mari-ann.einarsrud@ntnu.no

Graphical abstract

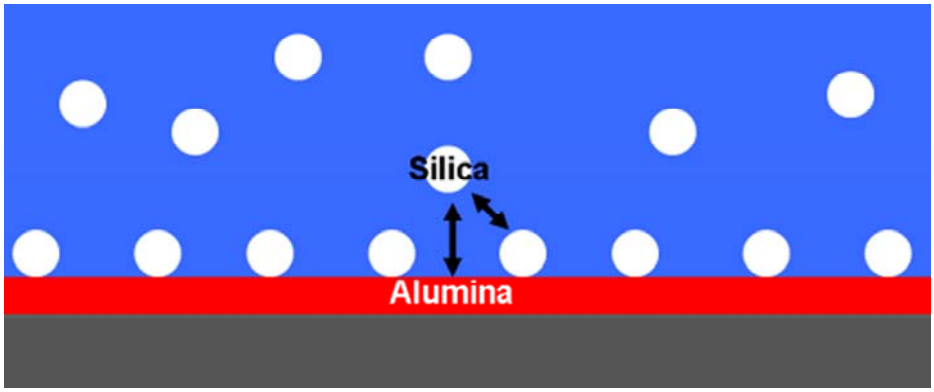

Optical reflectometry and a quartz crystal microbalance with dissipation detection studies showed that the surface coverage and formation of multilayers of silica nanoparticles on alumina was controlled by the electric diffuse double layer interactions between the substrate and the depositing particles.

Highlights

- Deposition of nanoparticles was monitored by optical and gravimetric techniques.
- Deposition behaviour monitored by independent techniques correlated well.
- Electron microscopy confirmed deposition behaviour.
- Surface coverage depended on differential levels of repulsive interactions.
- Multilayer of nanoparticles was deposited by eliminating repulsive interactions.

Abstract

Understanding of the interactions between particles and the substrate is important for successful sol-gel deposition of thin films. We have studied the deposition of silica nanoparticles on alumina coated surfaces in aqueous electrolytes by optical reflectometry (OR) and a quartz crystal microbalance with dissipation (QCM-D). The deposition of negatively charged silica nanoparticles on positively charged alumina was primarily controlled by the electric diffuse double layer interactions between the substrate and the deposited particles, modulated by the counter-ion release. The build up of a negative charge on the positively charged substrate resulted in a decrease in the deposition rate with increasing surface coverage. Higher surface coverage of silica nanoparticles was obtained at low pH than at high pH conditions, due to reduced electric diffuse double layer repulsion between the silica nanoparticles. The deposition was enhanced at high pH by increasing the concentration of NaCl due to compression of the electric diffuse double layer. In particular, the repulsion between the silica nanoparticles was efficiently screened at a concentration of NaCl higher than 100 mM and thick silica layers could be deposited at pH = 6 and 8.

Keywords: Optical reflectometry, QCM-D, Spectroscopic ellipsometry, Nanoparticles, Coatings, Colloidal silica, Sol–gel.

1. Introduction

Sol–gel processes are effective methods to coat surfaces and alter mechanical and chemical properties of different objects, in order to e.g. achieve resistance against corrosion and abrasion [1,2]. A potentially cost effective and environmentally benign sol–gel coating process is to deposit nanoparticles from an aqueous solution of colloidal silica. Indeed, deposition of silica nanoparticles from sols can be economically viable for large scale manufacturing practices. The main challenge with this approach is to be able to control the coverage and thickness of the deposited coatings and to avoid crack formation.

Sol-gel coatings are commonly prepared by dipping or spinning techniques that enhance the evaporation rate of the solvent and promote the formation of a dense particle gel onto the substrate, *i.e.* a type of sol-gel transition. However, these approaches are often limited by the collapse and cracking of the deposited particle gel because of the stresses induced primarily by the solvent removal [3-5]. The particle interactions have a pivotal influence on the sol-gel transition, and it has been shown that deposition of crack free silica coatings could potentially be achieved by altering the pH and concentration of salt [3-7].

Deposition of particles onto various substrates from liquid dispersions, has been studied by both direct and indirect experimental techniques [8]. From aqueous sols such depositions has been directly studied by *in situ* optical microscopy coupled with image analysis [8], which is appropriate for colloids larger than the wavelength of light. Microscopic techniques that require a vacuum atmosphere are truly difficult to interface with liquid environments, and also mechanical probes seem to have drawbacks for *in situ* imaging of loosely attached nanoparticles in the liquid environments. It has been shown that gravimetric methods can be utilised to monitor the deposition behaviour of silica nanoparticles at different concentration of NaCl and pH [9-11]. A quartz crystal microbalance with dissipation detection (QCM-D) is

very sensitive to mass changes and can be used in liquid solutions. Although both mass and dissipation are composite measures that include effects of solvent as well as nanoparticles, QCM-D has been used to monitor deposition of nanoparticles [12-16], also in combinations with combinatorial protocols [17].

The deposition of nanoparticles can also be studied by optical reflectometry (OR) [16,18-21] where the reflecting substrate carries a thin dielectric layer [22]. Böhmer *et al.* used OR to study how the size and concentration of silica nanoparticles and the ionic strength affected the deposition onto polyelectrolyte-coated substrates [19-21]. The initial deposition rate increased with decreasing particle size and increasing particle concentration [19,20]. They also showed that while the deposited amount of nanoparticles and surface coverage increased with increasing concentration of NaCl, the initial deposition rate remained unaffected [19,20]. Böhmer *et al.* did not study the effect of pH on the deposition of the silica nanoparticles because the adsorption and desorption behaviour of the polyelectrolyte would have been pH dependent [23,24]. An alternative method for attracting nanoparticles of silica to surfaces is to coat silicon wafers by oxides with various isoelectric points. Huynh *et al.* used substrates coated with titania and observed deposition and detachment of silica nanoparticles by OR [25].

Xu *et al.* combined QCM–D and OR to investigate how the particle concentration affected the kinetics of silica nanoparticle deposition on surfaces coated with polyelectrolytes at a pH = 10.5 [16]. They showed that by increasing the concentration of nanoparticles, the deposition rate increased [16], and also deduced that structural changes developed after the nanoparticles were deposited, by analysing the change of the dissipation characteristics during the QCM-D measurements.

In this study, we have investigated the deposition of negatively charged silica nanoparticles on positively charged alumina coated substrates by a combination of OR and QCM-D. The

electrostatic interactions between the particles and the substrate were controlled by systematically varying pH and ionic strength of the electrolyte. QCM-D was also used for observing variations in the viscoelastic behaviour of the deposited nanoparticle layer by monitoring dissipation. SEM and spectroscopic ellipsometry were used to determine the surface coverage and thickness of the layers deposited during the OR measurements.

2. Materials and methods

2.1. Materials

Aqueous colloidal sols of silica (Bindzil 30/220, EKA Chemicals, AB) were used to study the deposition of nanoparticles, and the properties of the sol are presented in Table 1. Particle size (average hydrodynamic diameter) and polydispersity index were estimated through cumulants analysis of intensity autocorrelation function determined by PCS (Beckman Coulter N5 Submicron equipped with a 632 nm laser). Samples were filtered by 0.2 μm syringe filters before PCS measurements. The particle size distribution of the sols was determined to be broad as indicated by the polydispersity index in Table 1 and as shown in the SEM images of deposited films. The zeta potential of the silica nanoparticles was determined by electrophoresis (Malvern, Zetasizer Nano ZS). Fig. 1 shows that the isoelectric point of the silica nanoparticles is around pH_{IEP} = 2. Prior to the deposition experiments, the sols were diluted to 0.1 wt. % by mixing with deionised water. The concentration of NaCl and pH of the sols were adjusted by addition of analytical grade NaCl, NaOH and HNO_3. Also, aqueous solutions of NaCl, having the same pH as the diluted sols, were prepared. The refractive index (n) of the solutions of NaCl and the diluted sols of silica particles were measured with a refractometer (RE 50, Mettler Toledo) and no difference between refractive indices of the diluted sols and the NaCl solutions was recorded.

Silicon wafers (111) with a diameter of 100 mm (WaferWorld Inc.) were used as substrates. The surface of the wafers were oxidised thermally in air, which produced a silica layer of 110 nm. The oxidised wafers were coated by sputtering with 12 nm thick alumina by applying 500 W RF power in 0.4 Pa argon atmosphere for 12 min to create a positive charge of the surface of the wafers at the investigated pH-values. Atomic force microscopy (AFM) was used to determine the roughness of the as-sputtered oxidized silicon substrate surface (R_{RMS}=0.2 nm) in contact mode. The wafers were cut to 40 x 10 mm and cleaned by treatment in UV/ozone for 20 min before the OR experiments.

Quartz crystals (5 MHz, AT-cut) coated with 100 nm thick alumina layers (Q-Sense) were used as substrates during the QCM-D measurements. The quartz crystals were cleaned by treatment in UV/ozone for 20 min before the experiments.

2.2. Optical reflectometry

The principle of OR has been explained elsewhere [20,22,24,26,27]. The effect of experimental parameters on the deposition of silica nanoparticles can be evaluated by determining the normalised reflectometry signal

$$\frac{S - S_o}{S_o} = \frac{\Delta S}{S_o} \qquad (1)$$

where S is the reflectometry signal and S_o is the baseline measured before the deposition of the nanoparticles. The OR measurements were performed using a stagnation-point flow cell and He-Ne laser (wavelength 633 nm) as described elsewhere [24,26,27]. The measurement cell (made of quartz) was cleaned by injecting a dilute solution of H_2SO_4 and rinsed with large amounts of deionised water before placing the substrate in the cell. A representative injection sequence used for the measurements is presented in Fig. 2. First, a solution of NaCl with

identical pH and concentration of NaCl as the sol was injected into the cell for 15 min (stage 1). Afterwards, the sol was injected for 30 min (stage 2), followed by re-injection of the solution of NaCl for 10 min (stage 3). The pH was varied from 2 to 8, and the concentration of NaCl was varied from 1 mM to 1000 mM at a fixed pH = 8. Each measurement was repeated 2-3 times with a reproducibility of ~10 % as shown in Fig. 2. Although a sudden increase was observed immediately after the injection of the sol at the second stage, the signal decreased throughout all injection stages. The reflectometry signal can be affected by any variation occurring on the surface of the substrate: nanoparticle deposition and detachment, substrate oxidation or dissolution. The signal decrease during the first stage has been confirmed by injecting a solution of NaCl (1 mM) at pH = 5.5 and 8 for longer time intervals (results not shown). This trend was observed at a higher rate at pH = 8 than at lower pH. Degradation of the thin alumina film could contribute to the variation of the reflected light intensity during sequential injection of the NaCl solution and the sol. To compensate for these effects, the reflectometry signal (S) was corrected by determining $\Delta S/\Delta t$ at stage 1. Since the degradation was dependent on the pH of the solution, correction was carried out for each measurement independently.

2.3 Quartz crystal microbalance with dissipation

QCM-D measurements were carried out with a Q-Sense E1 system (Q-Sense) using the same injection sequence as for the OR measurements. Measurements were performed using a parallel plate flow cell. The injection of the silica nanoparticles was preceded by injection of the solvent to obtain the baseline developing due to the mass of the NaCl solution coupling with the quartz crystal. The flow rate was adjusted to 10 µL/min and enough time was allowed to obtain a flat baseline during injection of the NaCl solution. Unlike for the reflectometry measurements, a flat baseline was obtained in 20-25 min before the sols were injected. The

pH was varied from 2 to 6 and the concentration of NaCl from 1 mM to 500 mM at a fixed pH = 6. A set of measurements was performed for each condition for the sol. Several overtones of the frequency change (Δf) and the dissipation change (ΔD) were recorded in order to evaluate changing mass and energy dissipation of the deposited layers, respectively. The Voigt model was used for to numerically estimate parameters from the frequency and dissipation curves (for all recorded overtones) as implemented in the software Q-Tools (Q-Sense).

2.4. Characterisation of the deposited layers

The deposited layers were characterised by spectroscopic ellipsometry and SEM (Thermal Field Emission (FE-SEM) type equipped with a Gemini column (Zeiss)) imaging after the OR measurements. Prior to characterisation, the substrates were rinsed with deionised water and dried with nitrogen gas of 6.0 grade. The thickness of the deposited layers was measured by a UVISEL-NIR ellipsometer (Horiba Jobin-Yvon) and evaluated in the DeltaPsi 2 software. The substrate surface was modelled as a stack of a layer of silica (110 nm thick) and a layer of alumina (12 nm thick) on a silicon wafer. The deposited silica nanoparticles were modelled as a mixture of silica and voids to account for the discontinuous coverage. The surface coverage was also examined by SEM using image analysis software (Esilab, Microvision Instruments).

3. Results and discussion

3.1. Optical reflectometry

Figure 3a shows that the deposition of silica nanoparticles onto the alumina-coated substrates results in strong change of the normalised reflectometry signal ($\Delta S/S_o$) that depends on both the pH and the concentration of NaCl of the dispersions. The increase of $\Delta S/S_o$ at a critical deposition time was abrupt for all pH values but the magnitude of the increase in $\Delta S/S_o$

became smaller when the pH was increased. Beyond this initial deposition stage, the signal continued to increase slowly until steady-state was reached. While the initial increase of $\Delta S/S_o$ was smaller at pH = 4.1 compared to pH = 2 and 2.9, $\Delta S/S_o$ eventually approached a similar value at all three pH-values after 30 minutes of deposition. Similar trends was evident at pH = 4.8 and 6.2 although the increase during the second stage was slower and the final $\Delta S/S_o$ was smaller for these dispersions compared to the dispersions deposited at lower pH-values. At the plateau of the $\Delta S/S_o$ curves, the smallest value for $\Delta S/S_o$ was obtained at the highest pH; pH = 8. The initial increase of $\Delta S/S_o$ was completed in only a few seconds and then stayed constant. However, the magnitude and the temporal evolution of $\Delta S/S_o$ for particle deposition at pH = 8 was strongly dependent on the ionic strength as shown in Fig. 3b. The initial increase in $\Delta S/S_o$ increases with the electrolyte concentration. Also, while no additional change of $\Delta S/S_o$ could be detected beyond the initial jump at low electrolyte concentration, a progressive increase of $\Delta S/S_o$ was observed throughout the 30 min injection time at concentrations of NaCl > 1 mM. This increase became significant especially at a concentration of NaCl $\geq$ 500 mM (Fig. 3b), where the final value of $\Delta S/S_o$ was even higher than the value obtained for deposition at low ionic strength at low pH (pH = 2 and 2.9) (Fig. 3a). Fig. 3 also shows that a tre-injection of the solution of NaCl (without the silica particles) does not result in a decrease in $\Delta S/S_o$ for any pH or electrolyte concentration except at pH = 2, where the decrease in the $\Delta S/S_o$ suggests that the deposited particle film is partly detached from the substrate.

3.2. Quartz crystal microbalance with dissipation

Fig. 4 presents the how pH and concentration of NaCl of the dispersions affects the QCM-D response during silica nanoparticle deposition. All systems displayed an abrupt decrease of the frequency at a specific time irrespective of the pH and ionic strength of the dispersion which shows that particles are depositing onto the substrates. However, the frequency decreased less

abruptly at pH = 6 (Fig. 4a), as compared to when the deposition takes place at a lower pH. Increasing the concentration of NaCl in the dispersions at pH = 6 (Fig. 4b) results in a significant increase of the magnitude of the frequency decrease, which was consistent with an enhanced deposition of nanoparticles. Indeed, the reflectometry data, in Fig. 3b also showed that the amount deposited increased with increasing NaCl concentration. The frequency levelled off after several minutes of deposition at all conditions except for the dispersion containing 500 mM NaCl at pH = 6 where the frequency decreased continuously for more than one hour. We attribute this effect to partial detachment of the deposited particle film, which also was shown in Fig. 4.

Fig. 5 shows how the total decrease in frequency (Δf) and increase of dissipation (ΔD) vary with pH and concentration of NaCl. The values for Δf and ΔD were determined from the third overtone of the quartz crystals, by subtracting the baseline value from the long-time steady-state values. Fig. 5 shows that both Δf and ΔD decreased with increasing pH for deposition at an electrolyte concentration of 1 mM NaCl. The QCM-D results suggest that the deposited layers dissipate more energy when the pH was decreased. Fig. 5 also shows that Δf and ΔD increase strongly with ionic strength for deposition from dispersions at pH = 6. The somewhat deviating behaviour at pH = 2 was discussed above. We did not observe any significant effect of a possible change in roughness of the substrates during the QCM measurements as has been reported by others [28, 29].

3.3. Microstructure of the deposited nanoparticle layers

SEM micrographs of deposited silica nanoparticles with a size of the primary particles of 5-30 nm are shown in Fig. 6. The micrographs show that the coverage of the deposited silica particles was homogeneous but varied significantly with both the pH and the concentration of NaCl applied during deposition. The SEM micrographs show that the highest surface

coverage is obtained at pH = 2.9 as compared with both pH = 2.0 and pH = 6.0 at 1 mM NaCl (Fig. 6a-c), which corroborate the results obtained from the OR and QCM-D measurements. The surface coverage increased with an increasing concentration of NaCl, when the silica particles were deposited at a pH 6 (Fig. 6d-f). We summarised the effects of pH and concentration of NaCl on the surface coverage by image analysis of the SEM micrographs and by ellipsometry in Fig. 7. The ellipsometry and image analysis of the SEM micrographs corroborated the interpretations of the OR and QCM-D results and showed that the surface coverage decreased with an increasing pH-value and increased (at high pH) with increasing electrolyte concentration.

The conditions of the sol also affected the thickness of the deposited layers. Fig. 8 shows the thicknesses of the deposited layers measured by ellipsometry as well as thicknesses estimated from the QCM-D measurements using the viscoelastic model (Fig. 5b). The effective density of the layers was calculated by taking ρ_{SiO2} = 2.2 g/cm^3, ρ_{water} = 1 g/cm^3 and using the surface coverage data determined by the image analysis of SEM micrographs. The results obtained by ellipsometry and QCM-D methods showed similar trends but the absolute values of the thickness of the deposited layers were slightly different. However, the thickness of the deposited layers given in Fig. 8 was in agreement with the particle/aggregate sizes measured by PCS (Table 1). Increasing the concentration of NaCl in the dispersion induced deposition of multilayers with an estimated thickness of 75 nm at pH = 6 and 8 (Fig. 8).

3.4. Analysis of the deposition kinetics

The results of the time-dependent reflectometry (Fig. 3) and QCM-D (Fig. 4) measurements showed that initial rapid deposition of the silica nanoparticles was followed by a second,

slower deposition stage. The initial short term deposition stage was evaluated by using the frequency change recorded from the third overtone during the QCM-D measurements as a measure of deposition. The frequency change (f) exhibited a power law dependence on time (t) as given below [30]:

$$f = \alpha t^{\gamma} \qquad (2)$$

where the prefactor α and the power law exponent γ are system dependent parameters. Such a power law dependence between deposition and time has been developed by Magan et al. [30] by an extension of the Brownian Dynamics Simulation model to include particles interacting through DLVO potentials. The transition from the short term initial stage to the following slow deposition regime occurred at the total frequency decrease, Δf, reached 65 or 75 % of its maximal value. Although the exact transition time point depended on the conditions of the dispersion, a power law kinetics was always valid until 65 % of Δf was reached. This region was used for the analysis. By relating the frequency decrease (Fig. 4a) to the reflectometry data (Fig. 3a) and direct observations of monolayer coverage using SEM (Fig. 6b) and ellipsometry (Fig. 7a), it was possible to assign a Δf of 148 Hz to the formation of a dense monolayer of silica nanoparticles. We have used this value for the analysis of deposition kinetics. The parameters α and γ were determined by non-linear regression of the time-dependent data to the model function (Eq. 2) until 65 % of Δf was reached. The parameters determined by the non-linear regression are summarized in Table 2 together with the relevant properties of the dispersion. The prefactor α increased when the pH of the sol containing 1 mM NaCl increased but decreased with increasing concentration of NaCl at pH = 6. On the other hand, γ increased when the pH of the sol containing 1 mM NaCl increased from 2 to 3 and then, tended to decrease with increasing the pH from pH = 3 to 6. At pH = 6, γ increased when the concentration of NaCl of the sols increased from 1 to 100 mM.

Deposition of silica nanoparticle coatings onto alumina substrate involves interaction of the charged nanoparticles with the (oppositely) charged substrate where they deposit. The nanoparticles of silica attained a negative charge by deprotonation at pH > 2 (Fig. 1), and for alumina surfaces such deprotonation occurred at pH > 8 [31]. Thus, alumina surfaces and silica nanoparticles have surface charges with opposite sign between pH = 2 and 8 and thus experience an attraction by electric diffuse double layer interactions [32]. We have made an attempt to relate the parameters α and γ in Table 2 to the balance of attraction and repulsion between the substrate and the depositing silica particles as a function of pH and concentration of NaCl. The increase in the prefactor α with increasing the pH from 2 to 4.2, may have been related to an increased magnitude of the electric diffuse double layer attraction [19]. Please note that the prefactor α did not increase beyond a value of about 0.5 when the pH was increased from 4.2 to 6; this increase suggested that the deposition was diffusion controlled under these conditions and a further increase of the electric diffuse double layer attraction would have a minor effect on the deposition kinetics. An increase in the ionic strength (from 1 to 100 mM NaCl at pH=6) resulted in a decrease in α, which can be related to a decrease in both the range and magnitude of the electric diffuse double layer attraction. The decrease in the exponent γ with increase in pH from 3 to 6 of the sol containing 1 mM NaCl might be related to repulsive interactions between the incoming nanoparticles and the particle coated substrates becoming more prominent as the deposition progresses. However, at pH = 2, γ is smaller than at pH = 3, probably due to weak attraction (as implied by α in Table 2) and detachment of the silica nanoparticles from alumina surface during deposition (Fig. 4a). Thus, deposition of silica nanoparticles on the alumina surface is initially maintained by electric diffuse double layer attraction unless it is obstructed by pre-deposited particles reversing the sign of the zeta potential on the surface [19]. By increasing the pH in the silica dispersion containing 1 mM NaCl, a thick electric diffuse double layer surrounding the deposited

nanoparticles effectively prevents further deposition. Increasing the ionic strength from 1 to 100 mM NaCl (at pH = 6) resulted in an increase in the power law exponent (γ), which could be related to a decrease in both the range and magnitude of the electric diffuse double layer repulsion.

4. Conclusion

The deposition and surface coverage of silica nanoparticles on an oppositely charged alumina surface can be controlled by the pH and concentration of NaCl. Homogeneous deposition with the highest surface coverage was obtained for dispersion with an intermediate pH (pH = 2.9), while the degree of coverage decreased while increasing the pH > 6. At this higher pH range the deposition of nanoparticles was enhanced when the electric diffuse double layer repulsion was weakened by increasing the concentration of NaCl above 100 mM. Aggregation of primary nanoparticles and multilayer deposition was induced when the range of the electric diffuse double layer repulsion was decreased by an increase in electrolyte concentration. The obtained understanding of the deposition parameters influence on the deposition rate and film thickness and degree of coverage gives guidelines for a successful sol-gel deposition of silica thin films.

Acknowledgement

This work was financially supported by The Research Council of Norway (NANOMAT, grant number 182033/S10). The authors would like to thank Professor Tor Grande for his valuable comments. The authors would also like to thank EKA Chemicals for supplying silica sols, Researcher Marit Stange for sputtering the alumina layer on the Si wafers and FEMTO-ST

Institute (R. Salut) for granting access to the electron microscope facility of the MIMENTO technology platform.

References

[1] G. Schottner, Chem. Mater. 13 (2001) 3422-3435.

[2] D. Wang, G.P. Bierwagen, Prog. Org. Coat. 64 (2009) 327-338.

[3] R.K. Iler, The chemistry of silica. Wiley, New York, 1979.

[4] J.C. Brinker, G.W. Scherer, Sol-gel science: The physics and chemistry of sol-gel processing. Academic Press, London, 1990.

[5] J.C. Brinker, G.C. Frye, A.C. Hurd, C.S. Ashley, Thin Solid Films, 201 (1991) 97-108.

[6] G.W. Scherer, J.C. Brinker, in: H.E. Bergna, W.O. Roberts (Eds.) Colloidal Silica Fundamentals and Applications, CRC Press, Boca Raton, 2006, p. 613.

[7] A.J. Hurd in: H.E. Bergna, W.O. Roberts (Eds.), Colloidal Silica Fundamentals and Applications, CRC Press, Boca Raton, 2006, p. 653.

[8] Z. Adamczyk, Adv. Colloid Interface Sci. 100 –102 (2003) 267-347.

[9] R.P. Socha, J. Fransaer, Thin Solid Films 488 (2005) 45-55.

[10] R. Socha, N. Pommier, J. Fransaer, Surf. Coat. Techol. 201 (2007) 5960-5966.

[11] H. Guleryuz, I. Kaus, C. Filiàtre, T. Grande, M-A. Einarsrud, J. Sol-Gel Sci. Technol. 54 (2010) 249-257.

[12] A. Krozer, S.A. Nordin, B. Kasemo, J. Colloid Interface Sci. 176 (1995) 479-484.

[13] J.J. Park, S.H. De Paoli Lacerda, S.K. Stanley, B.M. Vogel, S. Kim, J.F. Douglas, D. Raghavan, A. Karim, Langmuir 25 (2009) 443-450.

[14] J. Fatisson, R.F. Domingos, K.J. Wilkinson, N. Tufenkji, Langmuir 25 (2009) 6062-6069.

[15] D. Xu, C. Hodges, Y. Ding, S. Biggs, A. Brooker, D. York, Langmuir 26 (2010) 8366-8372.

[16] D. Xu, C. Hodges, Y. Ding, S. Biggs, A. Brooker, D. York, Langmuir 26 (2010) 18105-18112.

[17] G. Wang, M. Rodahl, M. Edvarsson, S. Svedhem, G. Ohlsson, F. Höök, B. Kasemo, Rev Sci. Instrum. 79 (2008) 075107.

[18] J. Kleimann, G. Lecoultre, G. Papastavrou, S. Jeanneret, P. Galletto, G.J.M. Koper, M. Borkovec, J. Colloid Interface Sci. 303 (2006) 460-471.

[19] R.A. Hayes, M.R. Böhmer, L.G.J. Fokkink, Langmuir 15 (1999) 2865-2870.

[20] M.R. Böhmer, E. van der Zeeuw, G.J.M. Koper, J. Colloid Interface Sci. 197 (1998) 242-250.

[21] M.R. Böhmer, J. Colloid Interface Sci. 197 (1997) 251-256.

[22] J.C. Dijt, M.A. Cohen Stuart, G.J. Fleer, Adv. Colloid Interface Sci. 50 (1994) 79-101.

[23] B. Cabot, A. Deratani, A. Foissy, Colloids Surf., A 139 (1998) 287-297.

[24] T. Roques-Carmes, F. Membrey, C. Filiatre, A. Foissy, J. Colloid Interface Sci. 245 (2001) 257-266.

[25] L. Huynh, A. Feiler, A. Michelmore, J. Ralston, P. Jenkins, Miner. Eng. 13 (2000) 1059-1069.

[26] C. Buron, C. Filiâtre, F. Membrey, A. Foissy, Colloids Surf., A 289 (2006) 163-171.

[27] C. Buron C, C. Filiâtre, F. Membrey, H. Perrot, A. Foissy, J. Colloid Interface Sci. 296 (2006) 409-418.

[28] E. Tellechea, D. Johannsmann, N.F. Steinmetz, R.P. Richter, I. Reviakine, Langmuir 25 (2009) 5177-5184.

[29] M. Urbakh, L. Daikhin, Phys. Rev. B 49 (1994) 4866-4870.

[30] R.V. Magan, R. Sureshkumar, J. Colloid Interface Sci. 297 (2006) 389–406.

[31] Kosmulski, J. Colloid Interface Sci. 298 (2006) 730-741.

[32] J. Israelachvili, Intermolecular and surface forces, Elsevier, Amsterdam, 2010.

Table captions

Table 1 Properties of the original silica sol.

Table 2 Effect of pH and concentration of NaCl on the initial deposition kinetics and the parameters determined by fitting process.

Figure captions

Fig. 1. Effect of pH on zeta potential of the silica nanoparticles. The line is a guide to the eye.

Fig. 2. Variation of the reflectometry output (S) during the injection sequence applied for the OR measurements. At stage 1, a NaCl solution having the same pH and concentration as the sol was injected into the cell. Injection of the sol started at stage 2. Re-injection of the NaCl solution started at stage 3.

Fig. 3. Effect of (a) pH (for the sol containing 1 mM NaCl) and (b) Concentration of NaCl (at pH = 8) on the normalised reflectometry output during deposition of silica nanoparticles. Normalised reflectometry output was calculated after correcting the reflectometry output recorded during injection of NaCl solutions and silica sols. Initiation of the third stage of injection is highlighted by arrows. An offset of 100 s was applied on abscissa to separate the initial part of the curves.

Fig. 4. Effect of (a) pH (for the sol containing 1 mM NaCl) and (b) Concentration of NaCl (at pH = 6) on the frequency decrease during deposition of silica nanoparticles. The frequency decrease measured from the third overtone of the quartz crystal during the QCM-D measurements. Initiation of the third stage of injection is highlighted by arrows. An offset of 50 s was applied on abscissa to separate the initial part of the curves.

Fig. 5. Effect of pH and Concentration of NaCl on (a) frequency change (Δf) and (b) dissipation change (ΔD) measured after 30 min sol injection (the end of the second injection stage) during QCM-D measurements. Δf and ΔD were determined from the third overtone of the quartz crystals by subtracting the baseline values from the final value measured at the end of stage 2 after 30 min of silica sol injection.

Fig. 6. SEM images of the deposited layers of silica nanoparticles at different sol conditions: (a) pH = 2, 1 mM NaCl, (b) pH = 2.9, 1 mM NaCl, (c) pH = 6.2, 1 mM NaCl, (d) pH = 8, 1 mM NaCl, (e) pH = 8, 100 mM NaCl, (f) pH = 8, 500 mM NaCl.

Fig. 7. Effect of (a) pH and (b) concentration of NaCl on surface coverage determined by SEM image analysis and ellipsometry. The lines are guides to the eye.

Fig. 8. Effect of pH and concentration of NaCl on the thickness of the silica layers deposited during reflectometry (measured by ellipsometry) and QCM-D (calculated according to viscoelastic modelling) measurements. The lines are guides to the eye.

Table 1

SiO_2 content (wt.%)	*Na_2O content (wt.%)*	*pH*	*Specific surface area (m^2/g)*	*Average particle size (hydrodynamic diameter) (nm)*	*Polydispersity index*
30	0.3	10.0	220	20 ± 8	0.45

Table 2

pH	*Concentration of NaCl (mM)*	Δf	*65 % of* Δf *(Hz)*	*Time interval (s)*	α	γ	R^2
2	1	122	79.3	69	0.168	1.538	0.9700
3	1	148	96.6	37	0.258	1.605	0.9847
4.2	1	127	82.2	31	0.507	1.500	0.9991
5	1	85	55.5	25	0.458	1.508	0.9950
6	1	68	44.3	32	0.552	1.345	0.9765
6	100	120	78.7	17	0.458	1.825	0.9884

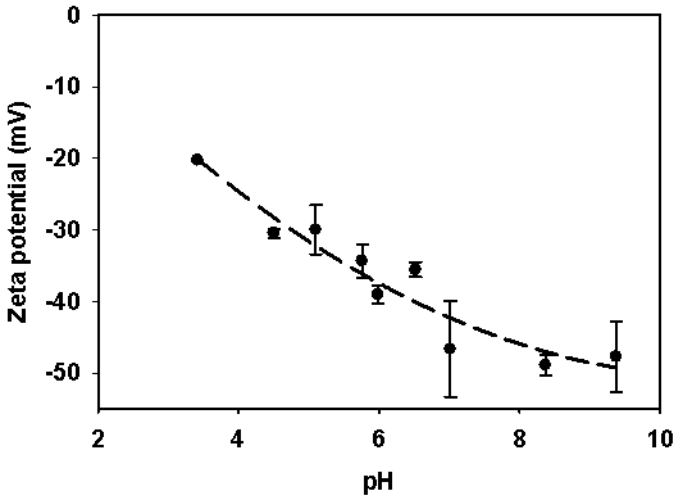

Fig. 1.

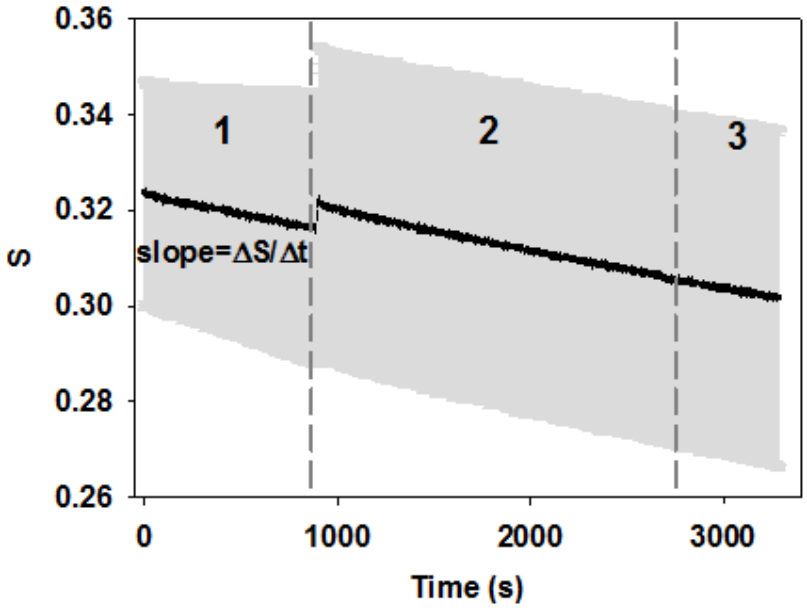

Fig. 2.

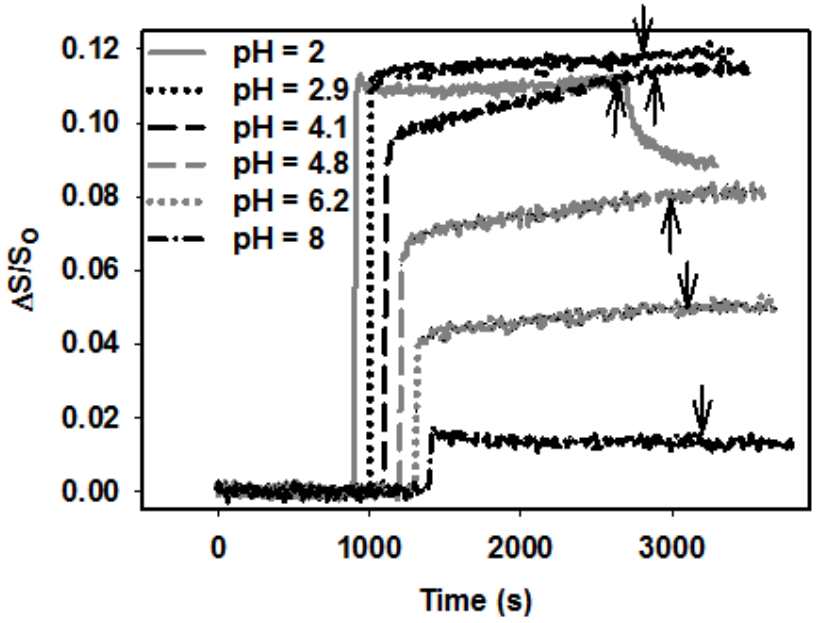
pH = 2
pH = 2.9
pH = 4.1
pH = 4.8
pH = 6.2
pH = 8
ΔS/S$_o$
0.12
0.10
0.08
0.06
0.04
0.02
0.00
0
1000
2000
3000
Time (s)

(a)

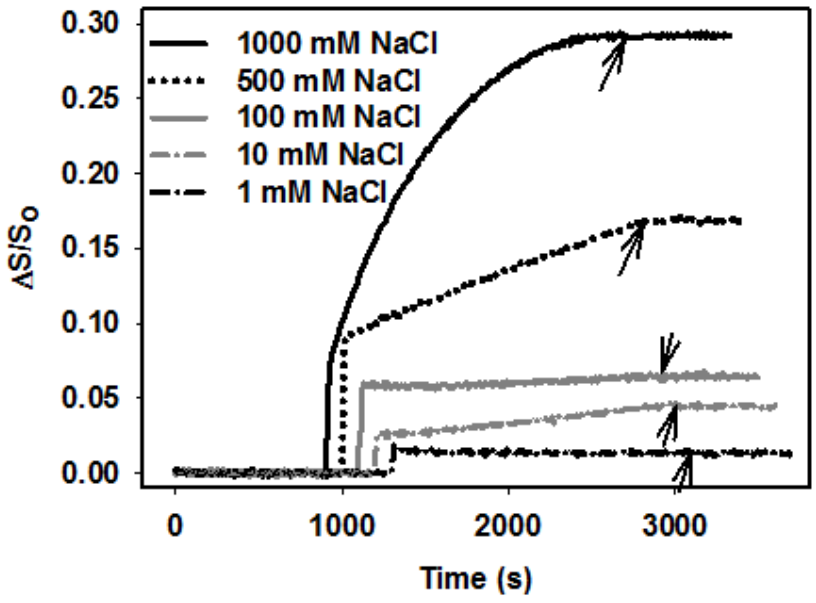
1000 mM NaCl
500 mM NaCl
100 mM NaCl
10 mM NaCl
1 mM NaCl
ΔS/S$_o$
0.30
0.25
0.20
0.15
0.10
0.05
0.00
0
1000
2000
3000
Time (s)

(b)

Fig. 3.

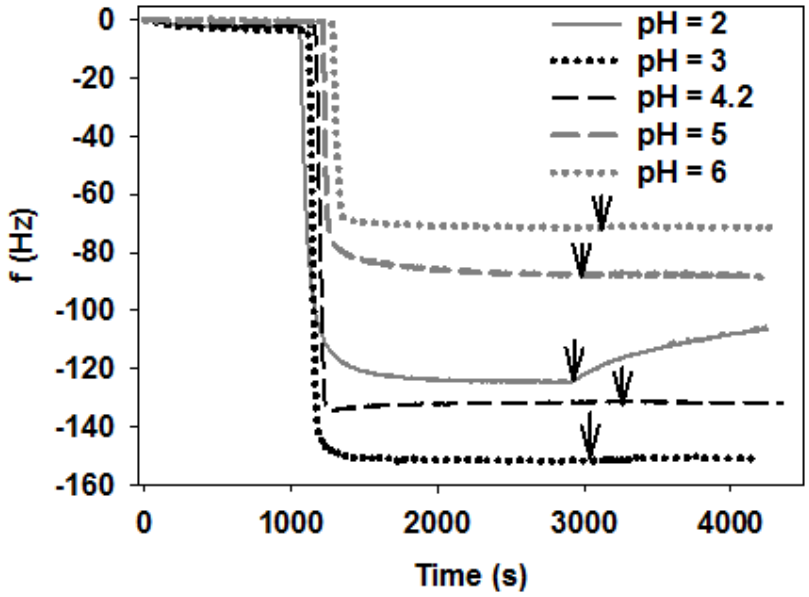
0
-20
-40
-60
-80
-100
-120
-140
-160
f (Hz)
0
1000
2000
3000
4000
Time (s)
pH = 2
pH = 3
pH = 4.2
pH = 5
pH = 6

(a)

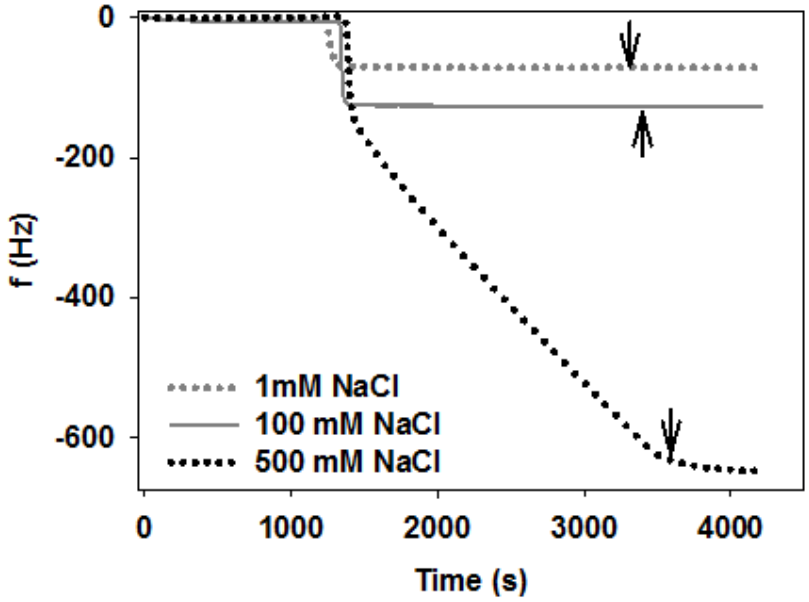
0
-200
-400
-600
f (Hz)
0
1000
2000
3000
4000
Time (s)
1mM NaCl
100 mM NaCl
500 mM NaCl

(b)

Fig. 4.

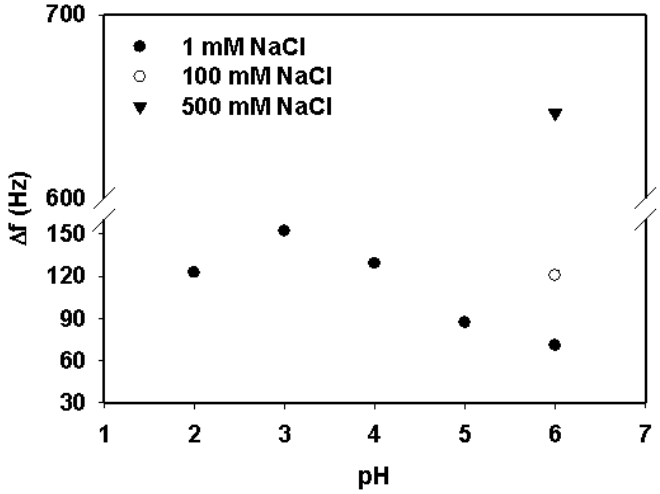
700
600
150
120
90
60
30
Δf (Hz)
1 mM NaCl
100 mM NaCl
500 mM NaCl
1
2
3
4
5
6
7
pH

(a)

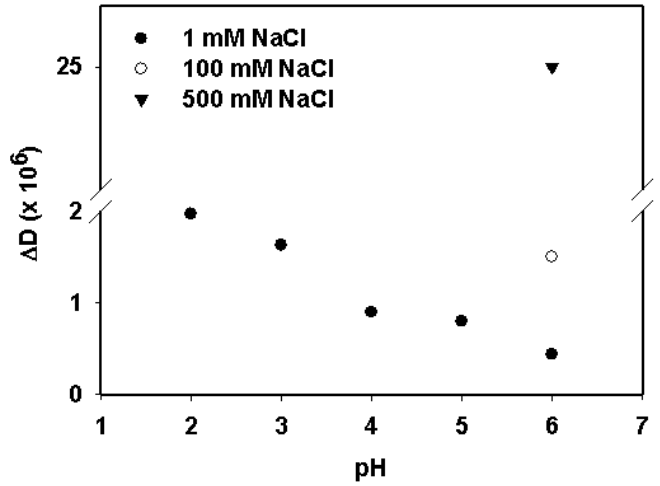
25
2
1
0
ΔD (x 10^6)
1 mM NaCl
100 mM NaCl
500 mM NaCl
1
2
3
4
5
6
7
pH

(b)

Fig. 5.

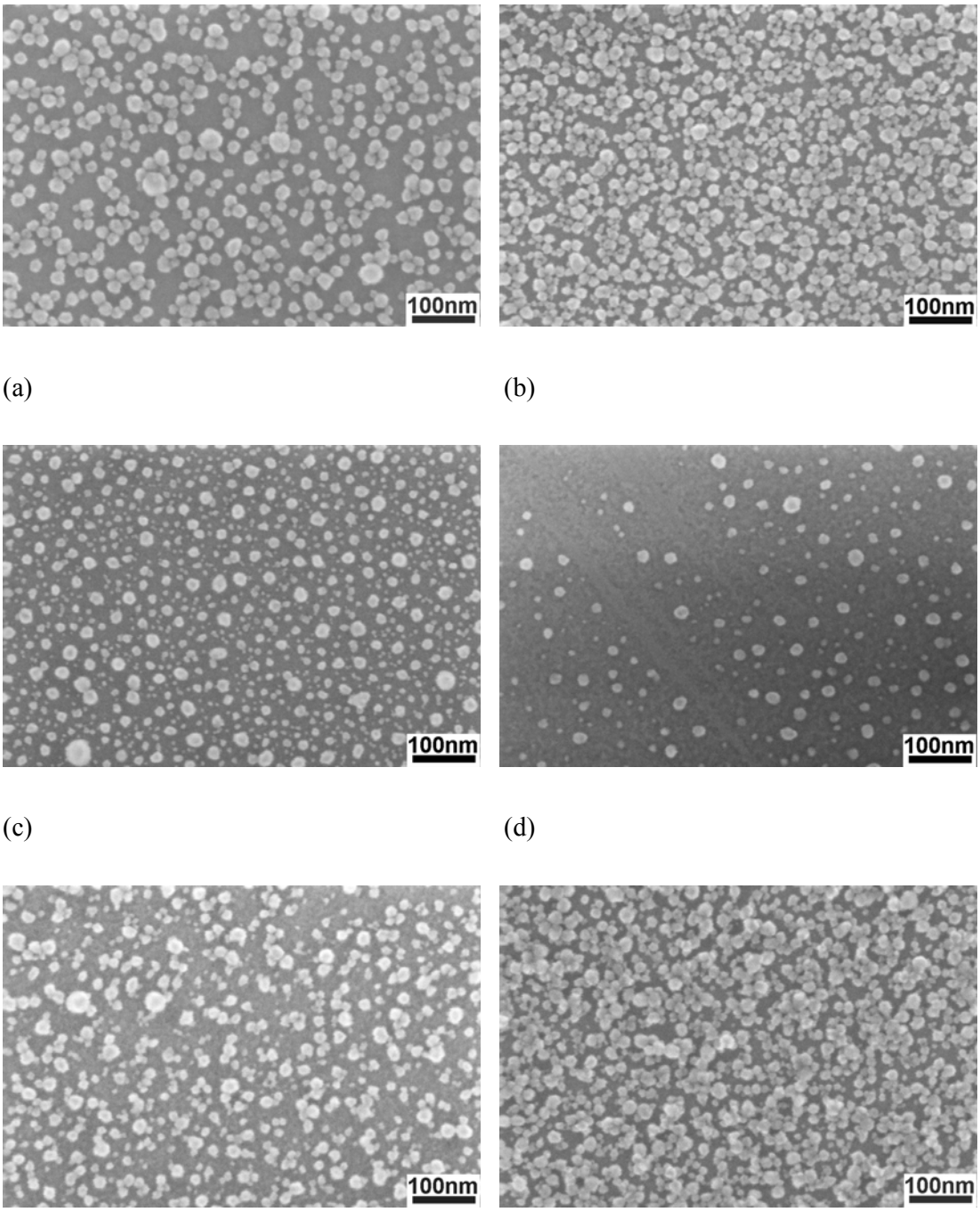

(a) (b)

(c) (d)

(e) (f)

Fig. 6.

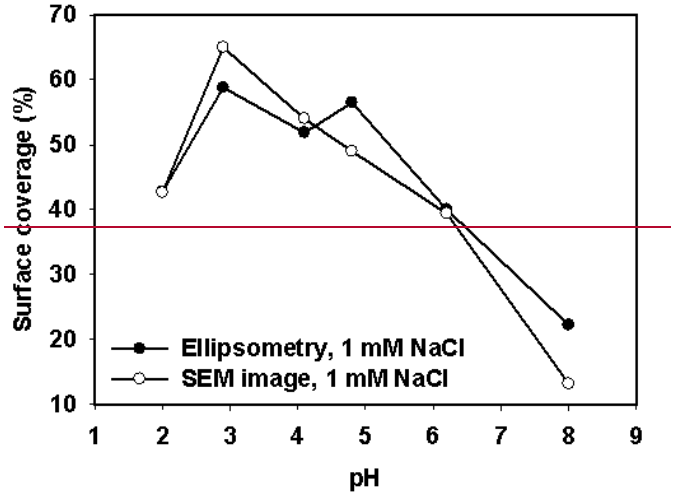
Surface coverage (%)
70
60
50
40
30
20
10
1
2
3
4
5
6
7
8
9
pH
Ellipsometry, 1 mM NaCl
SEM image, 1 mM NaCl

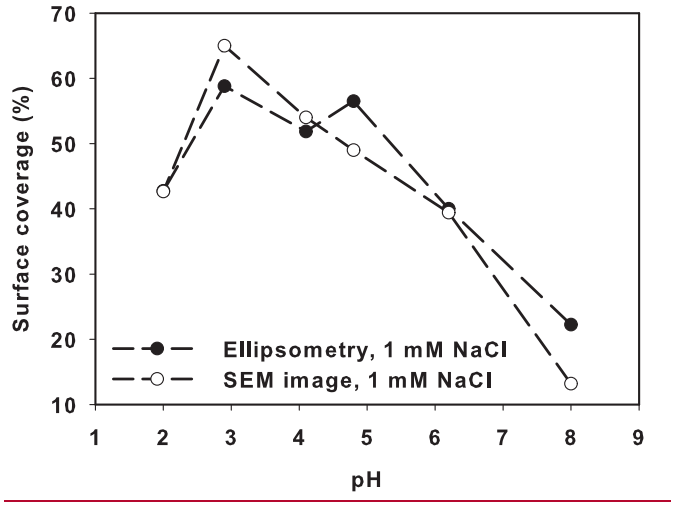
Surface coverage (%)
70
60
50
40
30
20
10
1
2
3
4
5
6
7
8
9
pH
Ellipsometry, 1 mM NaCl
SEM image, 1 mM NaCl

(a)

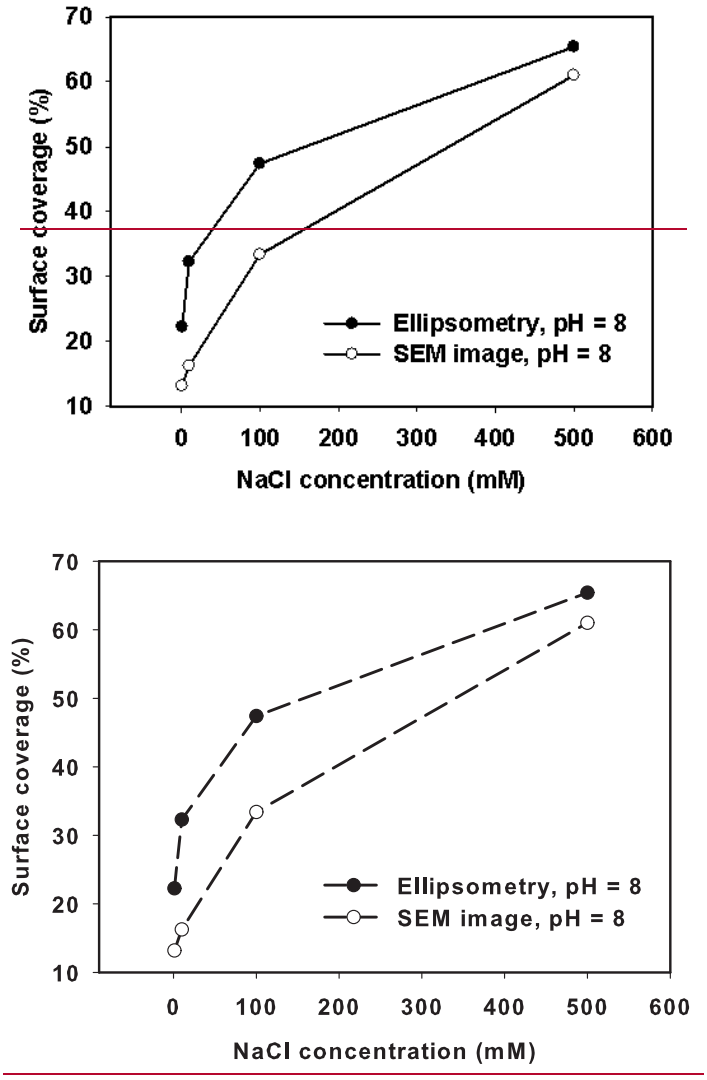
Surface coverage (%)
70
60
50
40
30
20
10
0
100
200
300
400
500
600
NaCl concentration (mM)
Ellipsometry, pH = 8
SEM image, pH = 8
Surface coverage (%)
70
60
50
40
30
20
10
0
100
200
300
400
500
600
NaCl concentration (mM)
Ellipsometry, pH = 8
SEM image, pH = 8

(b)

Fig. 7.

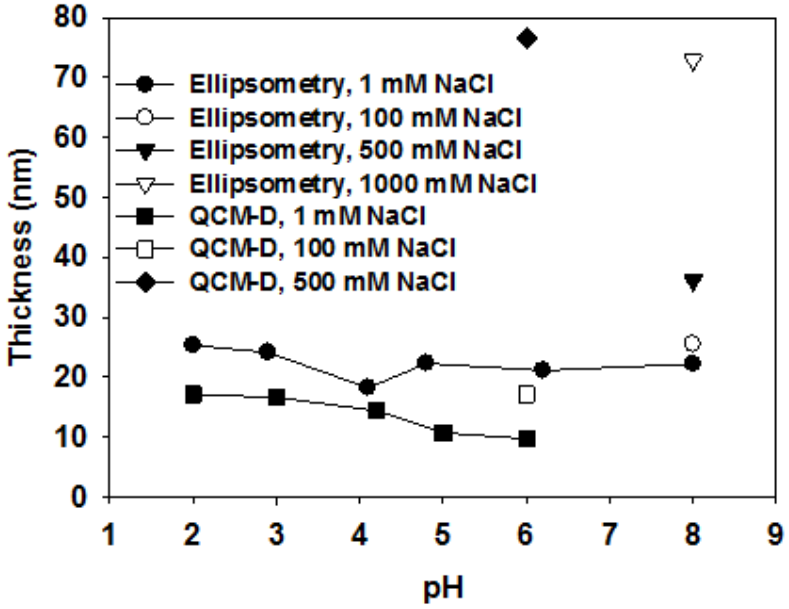
Thickness (nm)
pH
Ellipsometry, 1 mM NaCl
Ellipsometry, 100 mM NaCl
Ellipsometry, 500 mM NaCl
Ellipsometry, 1000 mM NaCl
QCM-D, 1 mM NaCl
QCM-D, 100 mM NaCl
QCM-D, 500 mM NaCl
0
10
20
30
40
50
60
70
80
1
2
3
4
5
6
7
8
9

Fig. 8.